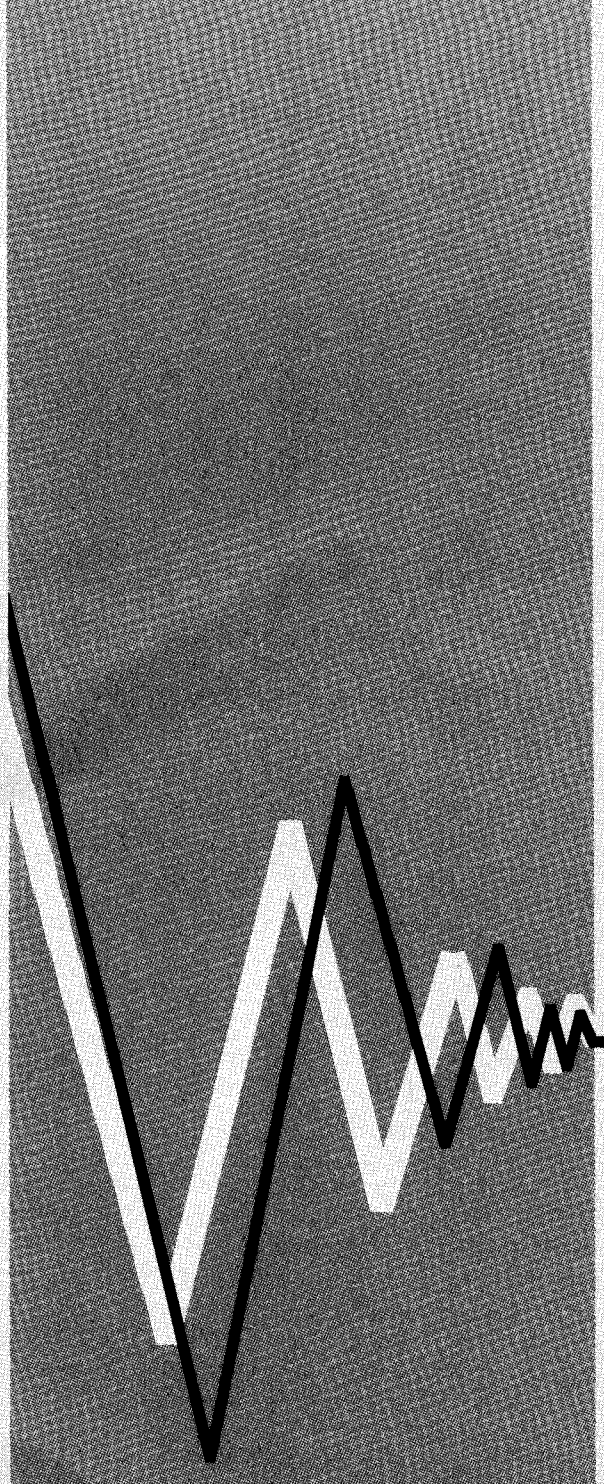

Online in 2001

Journal of INTELLIGENT MATERIAL SYSTEMS *and* STRUCTURES

VOL. 11, NO. 9 pp. 657–739 /SEPTEMBER 2000 ISSN: 1045-389X

The Use of Piezoceramic Transducers for Smart Structural Testing

BOR-TSUEN WANG* AND RONG-LIANG CHEN
Department of Mechanical Engineering, National Pingtung University of Science and Technology, Pingtung, Taiwan 91207, R.O.C.

ABSTRACT: This paper presents the use of piezoceramic transducers, Lead Zirconia Titanate (PZT) actuators and Polyvinylidene Fluoride (PVDF) sensors, for experimental modal testing of a simply supported plate. A series of rectangular-shaped PVDF films are evenly distributed over the plate and act as the sensing devices instead of traditional acceleration sensors. Pairs of rectangular PZT patches are bounded to opposite sides of the plate to form actuators and when they are excited by 180° out-of-phase stimulation, they will cause pure bending. The theoretical formulation of frequency response functions (FRFs) of the piezoceramic transducers is developed. The mode shape functions of the PZT actuator and the PVDF sensor are identified, respectively. Experiments are performed to obtain a column of FRF matrix. The structural modal parameters, including natural frequencies, modal damping ratios and mode shapes, can then be extracted by a modal parameter extraction method. Results show the modal parameters can be properly obtained and physically interpreted. This paper presents the concepts of smart structural testing (SST) with the use of piezoceramic transducers and leads to the applications of smart structures to health monitoring of structural systems.

INTRODUCTION

PIEZOCERAMIC transducers have been widely applied and integrated into structures for active structural vibration and acoustic control (Bailey and Hubbard, 1985; Plump, Hubbard and Bailey, 1987; Clark and Fuller, 1992; Clark, Burdisso and Fuller, 1993; D'Cruz, 1993; Young and Hansen, 1994; Wang, 1994). Many researches have been dedicated to the development of the PZT actuation models (Crawley and Luis, 1987; Dimitriadis, Fuller and Rogers, 1991; Im and Atluri, 1989; Wang and Rogers, 1991a; Wang and Rogers, 1991b; Gibbs and Fuller, 1992; Clark, Fuller and Wicks, 1991) as well as the PVDF sensing models (Hubbard, 1987; Lee and Moon, 1990; Collins et al., 1992; Collet and Jezequel, 1994; Tanaka, Snyder and Hansen, 1996) for beams and plates. Crawley and de Luis (1987) developed the PZT actuators adhered or embedded into cantilever beam for structural actuation. Dimitriadis et al. (1991) extended their work to two-dimensional plate problem and derived the actuation force model for PZT pure-bending excitation. Im and Atluri (1989) further considered the shear force and axial force effects for PZT actuator applied to beam structures. Wang and Rogers (1991a, 1991b) applied the classical laminate plate theory to model the embedded PZT actuator for beams and plates, respectively, considering pure-bending, pure-extension and asymmetric excitation modes. Gibbs and Fuller (1992) also derived the asymmetric PZT actuator excitation for beam structural vibration control.

The rectangular shape of PVDF film was introduced by Hubbard (1987) for the application to vibration control of beam structures as the sensor. Lee and Moon (1990) and Collin et al. (1992) developed special shape of PVDF film to sense the specific vibration modal response as known modal sensors. Collet and Jezequel (1994) and Tanaka et al. (1996) utilized the similar configuration of PVDF film as modal filters for vibration control. The applications of PZT actuator and PVDF sensor integrated with structures, so called smart structure system, to structural vibration and acoustic control is very promising.

The idea of smart structural testing is also of interest and leads to structural fault diagnosis and health monitoring (Galea, Chiu and Paul, 1993). Sun et al. (1994) derived the frequency response function (FRF) through electric admittance of piezoceramic transducers for obtaining the dynamic parameters of beam structures. However, they did not physically interpret those dynamic parameters. Norwood (1995) successfully applied both the impact hammer and PVDF film, respectively, as actuation sources for the modal testing of cylindrical shell structures. Wang (1996) derived the frequency response functions between the traditional and piezoceramic transducers for simply supported beam. He introduced the feasibility of the use of piezoceramic transducers for structural modal testing. Wang and Wang (1997) theoretically and experimentally demonstrated the rectangular shape of PZT actuator and PVDF sensor for cantilever beam modal testing. They showed that the system modal parameters, including natural frequencies, modal damping ratios and structural mode shapes, can be properly extracted. Wang (1998) further developed the modal analysis for the use of various forms of actuators and sensors. The FRFs can be derived and expressed in conventional modal format. The actuator and sensor mode shape functions are defined and interpreted according to types of actuators and sensors as well as the testing procedure.

*Author to whom correspondence should be addressed. E-mail: wangbt@mail.npust.edu.tw

1045-389X/00/09 0713-12 $10.00/0 DOI: 10.1106/P9GF-L9XT-FXCJ-CLBJ

This work intends to use the PZT actuator and PVDF sensor instead of traditional transducers, such as the impact hammer or shaker and accelerometer, for modal testing of simply supported plate. Huang et al. (1998) developed an identification algorithm base on modal equations for a thin plate using the piezoceramic transducers. They did extract the natural frequencies and modal damping ratios of the plate but not the structural mode shapes. This paper first develops the FRFs between the PZT actuator and PVDF sensor applied to the simply supported plate. The simply supported plate is constructed as Ochs and Snowdion (1975) suggested and has been shown for the correctness of the test structure by conventional modal testing (Wang and Chen, 1997). A series of rectangular shape of PVDF films are evenly distributed over the plate and act as the sensing devices instead of traditional acceleration sensors. Pairs of rectangular PZT patches are bounded to opposite sides of the plate to form actuators and when they are excited by 180° out-of-phase stimulation, they will cause pure bending. The testing procedure by fixing the PZT actuator location and roving the PVDF sensor location is adopted for experimental modal testing. A set of FRFs is measured and processed through modal parameter extraction method to determine the system modal parameters. Results show that modal frequencies, modal damping ratio and PVDF sensor mode shapes can be properly identified. In particular, for the simply supported boundary conditions the PVDF sensor mode shape is proportional to the displacement mode shape as demonstrated. The idea of smart structural testing is enhanced. The configuration of the system can also be applied to structural failure diagnosis.

THEORETICAL ANALYSIS

The thin plate theory is adopted, and the equation of motion for rectangular plate can be expressed as follows (Szilard, 1974):

$$D\nabla^2\nabla^2 w + \rho t_p \frac{\partial^2 w}{\partial t^2} + \bar{c}\frac{\partial w}{\partial t} = f(x, y, t) \tag{1}$$

where

$$D = \frac{E_p t_p^3}{12(1-\nu^2)} \tag{2}$$

$$\nabla^2 = \frac{\partial^2}{\partial x^2} + \frac{\partial^2}{\partial y^2} \tag{3}$$

To perform theoretical modal analysis, one can obtain the plate natural frequencies and their corresponding mode shapes for simply-supported boundary condition as follows (Szilard, 1974):

$$f_{mn} = \frac{\omega_{mn}}{2\pi} = \frac{\pi}{2}\left[\frac{m^2}{L_x^2} + \frac{n^2}{L_y^2}\right]\sqrt{\frac{D}{\rho t_p}} \tag{4}$$

$$\phi_{mn}(x, y) = \phi_m(x)\phi_n(y) = \sin\alpha_m x \sin\alpha_n y \tag{5}$$

where

$$\alpha_m = \frac{m\pi}{L_x} \tag{6}$$

$$\alpha_n = \frac{n\pi}{L_y} \tag{7}$$

Harmonic Analysis of PZT Actuator Excitation

Consider the actuation of the rectangular shape of PZT actuator as shown in Figure 1. Two PZT patches are adhered to the opposite sides of the plate symmetrically and activated 180° out-of-phase by a voltage input, V_c. The pure bending excitation can be activated. The equivalent force can be derived as distributed line moments along the four edges and expressed as follows (Dimitriadis, Fuller and Rogers, 1991):

$$\begin{aligned} f(x, y, t) = {} & M_{eq}\left[\delta'(x - x_{c_{1j}}) - \delta'(x - x_{c_{2j}})\right] \\ & \cdot \left[H(y - y_{c_{1j}}) - H(y - y_{c_{2j}})\right]e^{i\omega t} \\ & + M_{eq}[H(x - x_{c_{1j}}) - H(x - x_{c_{2j}})] \\ & \cdot [\delta'(y - y_{c_{1j}}) - \delta'(y - y_{c_{2j}})]e^{i\omega t} \end{aligned} \tag{8}$$

where

$$M_{eq} = C_0\Lambda \tag{9}$$

$$\Lambda = \frac{d_{31}}{t_c}V_c \tag{10}$$

The system response can also be harmonic and derived as follows:

$$w(x, t) = \sum_{m=1}^{\infty}\sum_{n=1}^{\infty} W_{mn}\phi_m(x)\phi_n(y)e^{i\omega t} \tag{11}$$

where

$$W_{mn} = \frac{-\left(\frac{1}{\alpha_m^2} + \frac{1}{\alpha_n^2}\right) \cdot M_{eq}[\phi_m'(x_{c_{2j}}) - \phi_m(x_{c_{1j}})][\phi_n'(y_{c_{2j}}) - \phi_n(y_{c_{1j}})]}{\left(\frac{L_x}{2}\frac{L_y}{2}\right)[D(\alpha_m^2 + \alpha_n^2)^2 - \omega^2\rho t_p + i\omega\bar{c}]} \tag{12}$$

$$\phi_m'(x_{c_{2j}}) - \phi_m'(x_{c_{1j}}) = -2\alpha_m \sin\left(\alpha_m \frac{l_{cx}}{2}\right)\phi_m(x_{c_j}) \tag{13}$$

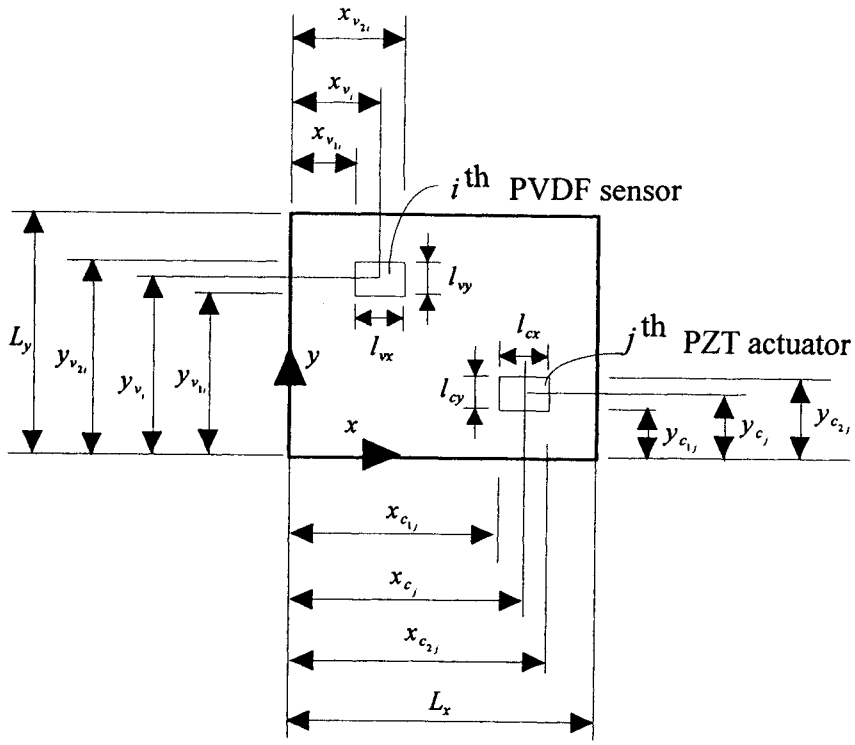

Figure 1. *The arrangement of the j-th PZT actuator and the i-th PVDF sensor on the rectangular plate.*

$$\phi_n'(y_{c_{2_j}}) - \phi_n'(y_{c_{1_j}}) = -2\alpha_n \sin\left(\alpha_n \frac{l_{cy}}{2}\right)\phi_n(y_{c_j}) \quad (14)$$

Equations (13) and (14) are the slope difference mode shape between two opposite edges of the PZT actuator and proportional to the displacement mode shape. For simply-supported boundary condition, the modal amplitude can also be expressed as follows:

$$W_{mn} = \frac{-4\alpha_m\alpha_n \sin\left(\alpha_m \frac{l_{cx}}{2}\right)\sin\left(\alpha_n \frac{l_{cy}}{2}\right) \cdot \left(\frac{1}{\alpha_m^2} + \frac{1}{\alpha_n^2}\right) M_{eq}\phi_{mn}(x_{c_j}, y_{c_j})}{\rho t_p \left(\frac{L_x}{2}\frac{L_y}{2}\right)[(\omega_{mn}^2 - \omega^2) + i2\xi_{mn}\omega_{mn}\omega]} \quad (15)$$

where

$$\phi_{mn}(x_{c_j}, y_{c_j}) = \phi_m(x_{c_j})\phi_n(y_{c_j}) \quad (16)$$

Harmonic Response of PVDF Sensor

The shape function of the i-th PVDF sensor as shown in Figure 1 can be defined as follows:

$$\Gamma(x, y) = \left[H(x - x_{v1_i}) - H(x - x_{v2_i})\right] \cdot \left[H(y - y_{v1_i}) - H(y - y_{v2_i})\right] \quad (17)$$

The PVDF film sensing equation can be derived as follows (Lee and Moon, 1990):

$$q(t) = \left(\frac{t_p + t_v}{2}\right)\int_0^{L_x}\int_0^{L_y}\Gamma(x, y)\left(e_{31}\frac{\partial^2 w}{\partial x^2} + e_{32}\frac{\partial^2 w}{\partial y^2} + 2e_{36}\frac{\partial^2 w}{\partial x \partial y}\right)dxdy \quad (18)$$

For the simply supported plate, torsional effect can be neglected, i.e., $e_{36} = 0$. The equation can be derived as follows:

$$q(t) = \left(\frac{t_p + t_v}{2}\right)e^{i\omega t}\sum_{m=1}^{\infty}\sum_{n=1}^{\infty} W_{mn}(e_{31}\alpha_m^2 + e_{32}\alpha_n^2)\frac{1}{\alpha_m^2}\frac{1}{\alpha_n^2} \cdot \{[\phi_m'(x_{v2_i}) - \phi_m'(x_{v1_i})][\phi_n'(x_{v2_i}) - \phi_n'(x_{v1_i})]\} \quad (19)$$

where

$$\phi_m'(x_{v2_i}) - \phi_m'(x_{v1_i}) = -2\alpha_m \sin\left(\alpha_m \frac{l_{vx}}{2}\right)\phi_m(x_{v_i}) \quad (20)$$

$$\phi_n'(y_{v2_i}) - \phi_n'(y_{v1_i}) = -2\alpha_n \sin\left(\alpha_n \frac{l_{vy}}{2}\right)\phi_n(y_{v_i}) \quad (21)$$

Again, the PVDF sensor mode shape is the slope difference mode shape and proportional to the displacement mode

shape for simply supported plate. The resultant voltage of the i-th PVDF sensor can be obtained as

$$V_{v_i}(t) = \frac{q(t)}{\varepsilon A_v} t_v \tag{22}$$

The resultant voltage can be rewritten as

$$V_{v_i}(t) = \frac{t_v}{\varepsilon A_v}\left(\frac{t_p + t_v}{2}\right) e^{i\omega t} \sum_{m=1}^{\infty}\sum_{n=1}^{\infty} 4\alpha_m \alpha_n W_{mn} \cdot \left[e_{31}\left(\frac{1}{\alpha_n}\right)^2 + e_{32}\left(\frac{1}{\alpha_m}\right)^2\right] \sin\left(\alpha_m \frac{L_{vx}}{2}\right) \cdot \sin\left(\alpha_n \frac{L_{vy}}{2}\right) \phi_{mn}(x_{vi}, y_{vi}) \tag{23}$$

Frequency Response Function

The frequency response function between the i-th PVDF sensor and the j-th PZT actuator can be derived and expressed in conventional modal format as

$$\alpha_{v_i f_j}(\omega) = \frac{V_{v_i}}{V_{c_j}} = \sum_{n=1}^{\infty}\sum_{m=1}^{\infty} \frac{\phi^v_{mn,i}\phi^c_{mn,j}}{(\omega^2_{mn} - \omega^2) + i(2\xi_{mn}\omega_{mn}\omega)} \tag{24}$$

where

$$\phi^c_{mn,j} = \frac{-4k_c\alpha_m\alpha_n\left(\frac{1}{\alpha_m^2} + \frac{1}{\alpha_n^2}\right)}{\sqrt{\rho t_p\left(\frac{L_x}{2}\frac{L_y}{2}\right)}} \cdot \sin\left(\alpha_m \frac{l_{cx}}{2}\right)\sin\left(\alpha_n \frac{l_{cy}}{2}\right)\phi_{mn}(x_{c_j}, y_{c_j}) \tag{25}$$

$$\phi^v_{mn,i} = \frac{4k_v\alpha_m\alpha_n\left[e_{31}\left(\frac{1}{\alpha_n^2}\right) + e_{32}\left(\frac{1}{\alpha_m^2}\right)\right]}{\sqrt{\rho t_p\left(\frac{L_x}{2}\frac{L_y}{2}\right)}} \cdot \sin\left(\alpha_m \frac{l_{vx}}{2}\right)\sin\left(\alpha_n \frac{l_{vy}}{2}\right)\phi_{mn}(x_{v_i}, y_{v_i}) \tag{26}$$

$$k_c = \frac{C_0 d_{31}}{t_c} \tag{27}$$

$$k_v = \frac{t_v}{\varepsilon A_v}\left(\frac{t_p + t_v}{2}\right) \tag{28}$$

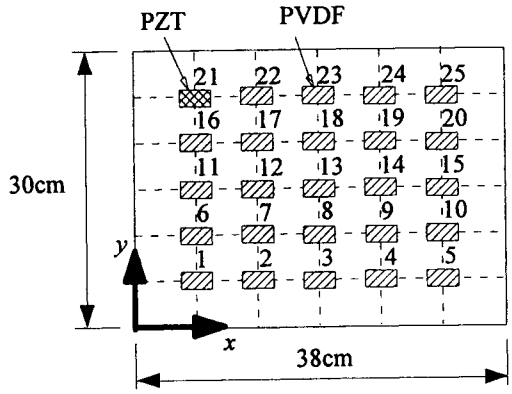

Figure 2. *The division and number of simply supported plate.*

In particular, both the PZT actuator and PVDF sensor mode shape functions (Wang, 1998) are the slope difference mode shapes. For simply supported boundary conditions, the slope difference mode shape is proportional to the displacement mode shape as shown in Equations (25) and (26).

EXPERIMENTAL ANALYSIS

The objective of experimental modal testing is to obtain the first four modes, i.e., $m = 2$ and $n = 2$. The grid of the plate is shown in Figure 2 and numbered up to 25 locations. The PZT actuator is located at position 21, while the PVDF sensors are evenly distributed at other positions. The test plate is shown in Figure 3. The test equipment layout is depicted in Figure 4, and the signal flow block diagram is also shown in Figure 5. White noise random signal from signal generator (BK3016) is input to voltage transformer (SQV3/500) and amplified about 90 times of voltage to be input to PZT actuator. The resultant voltage measured from the PVDF sensor is also amplified 90 times and input to channel B. Both channels are applied hanning windows to reduce leakages for random signals. The dual channel FFT analyzer (BK3550) captures both the input and output voltages of the PZT actuator and PVDF sensor, respectively, and calculates the frequency

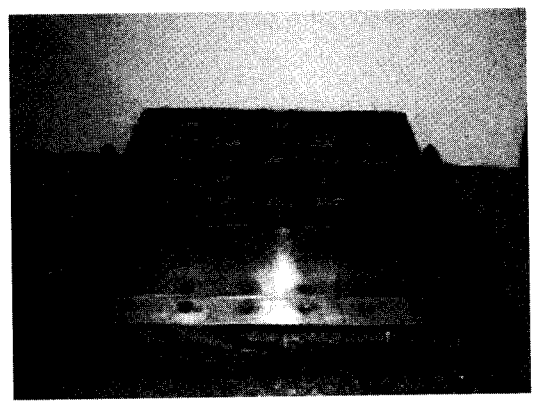

Figure 3. *The test plate.*

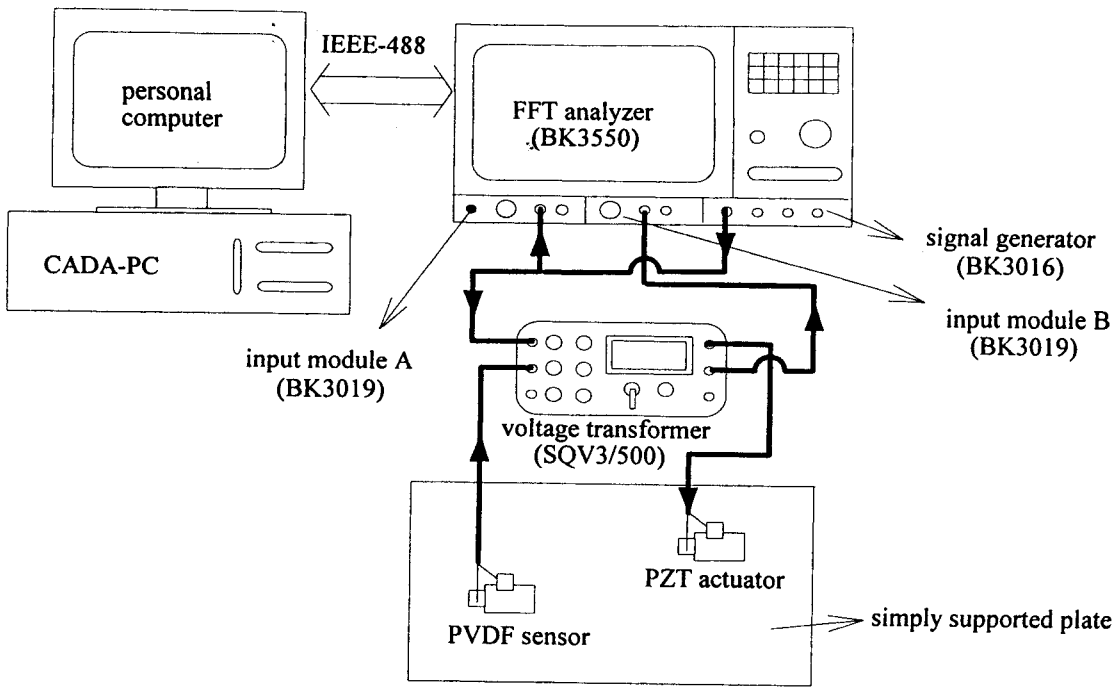

Figure 4. *Experimental equipment layout.*

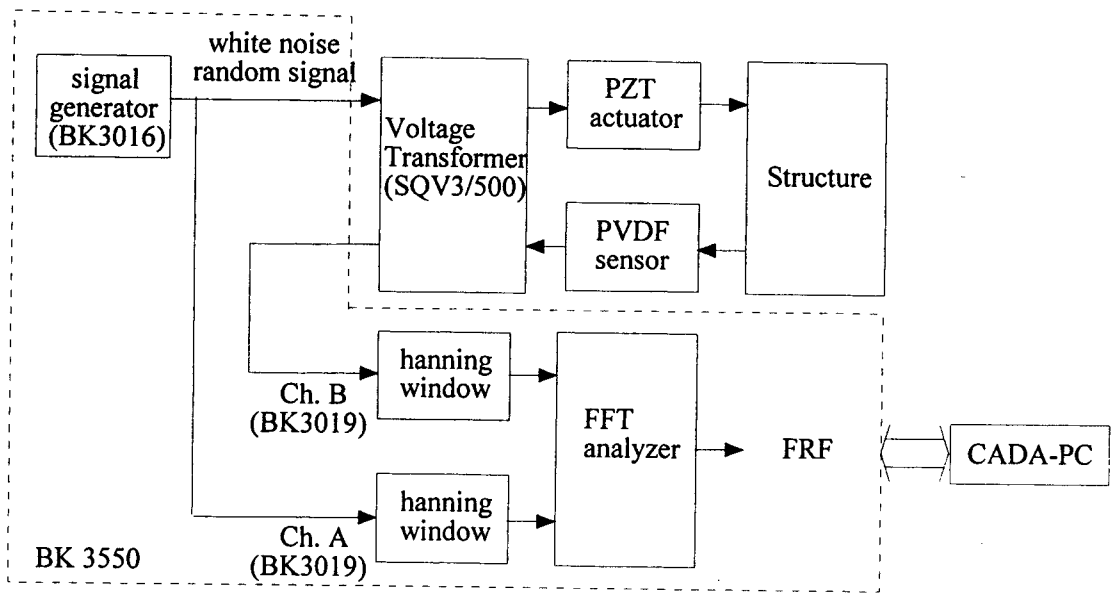

Figure 5. *Signal flow block diagram.*

response function (FRF) based on a hundred times of averages to reduce random errors. Let the PZT actuator be fixed, roving the PVDF sensors a total number of 25 sets of FRFs can be measured and transported to CADA-PC, a general purpose curve fitting software to extract the system modal parameters. Natural frequencies, modal damping ratios and PVDF mode shape functions of the simply supported plate can be extracted. The physical properties of the plate, PZT actuator and PVDF sensor are shown in Tables 1–3, respectively.

Table 1. Physical properties of plate.

Material	Steel
Length (L_x)	0.38 (m)
Width (L_y)	0.3 (m)
Thickness (t_p)	0.002 (m)
Density (ρ)	7870 (kg/m^3)
Young's modulus (E)	207×10^9 (N/m^2)
Poisson's ratio (ν)	0.292

Table 2. Physical properties of PZT actuator.

Type	G-1195
Length (l_{cx})	38 (mm)
Width (l_{cy})	19 (mm)
Thickness (t_c)	1.905 (mm)
Young's modulus (E_c)	6.3×10^{10} (N/m^2)
Density (ρ_c)	7650 (kg/m^3)
Poisson's ratio (ν_c)	0.28
Piezoelectric strain constant ($d_{31} = d_{32}$)	166×10^{-12} (m/V)

Table 3. Physical properties of PVDF sensor.

Type	DT1-028K
Length (l_{vx})	38 (mm)
Width (l_{vy})	19 (mm)
Thickness (t_v)	28×10^{-6} (m)
Young's modulus (E_v)	6.3×10^{10} (N/m^2)
Density (ρ_v)	1800 (kg/m^3)
Poisson's ratio (ν_v)	0.33
Piezoelectric field intensity constant ($e_{31} = e_{32}$)	54×10^{-3} (m/V)
Permittivity (ε)	106×10^{-12} (F/m)

RESULTS AND DISCUSSIONS

Verification of Frequency Response Functions

Figures 6(a) and 6(b) show the FRFs for $i=2, j=21$ and $i=16, j=21$ respectively. Because the PZT actuator is located at position 21, and both sides of the plate is adhered with the PZT patches, the 21st PVDF sensor is ignored. In this work, the FRF of $i=21, j=21$ is not available and replaced by that of $i=16, i=21$. In Figure 6, the solid line denotes the experimental FRF, the dash line denotes the synthesized FRF derived from the extracted modal parameters, and the chain line denotes the theoretical FRF. It should be noted that the synthesized FRF is based on the first four modes for identifying the first four modes of the plate. The higher modes appear to be close and reveal coupling effect. In higher frequency range, such as between 400–800 Hz as shown in Figure 6, there are at least 6 close modes. Those modes are not included in the synthesized FRF. One can observe that the synthesized FRF reasonably agrees with experimental FRF between 0 and 400 Hz. The 60 Hz electrical noise in experiments is eliminated. This indicates the correctness of curve fitting process. One can also observe that the resonance frequencies and the shape of FRFs show reasonable agreement between the theoretical and experimental FRFs. The extremely low value in the low frequency range for both experimental and synthesized FRFs may come from the effect of grounded spring stiffness from the simulated simply supported boundary. The large difference in amplitudes between the theoretical and experimental FRFs may be due to the imperfect bonding effect of PZT patches and PVDF films. Both the PZT actuation and PVDF sensing models are based on ideal bonding neglecting the adhesive and mass effects of piezoelectric transducers. However, from the point of view in structural testing, the shape of FRF is far more important in order to extract the modal parameters than the amplitude. On the other hand, more sophisticate models including adhesive layer effect for PZT actuation and PVDF sensing models may be necessary and interested. The coherence functions corresponding to experimental FRFs in Figure 6 are shown in Figure 7. Most values are near 0.9 except where the anti-resonance frequencies and 60 Hz harmonics occur. The small value of coherence function at low frequency range can be the boundary effect due to the limitation of dynamic range of FRF analyzer. Generally speaking, the

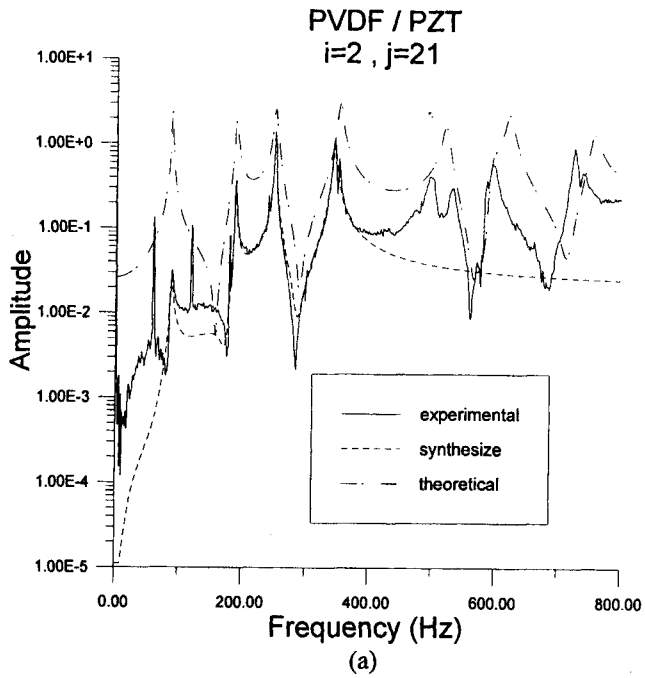

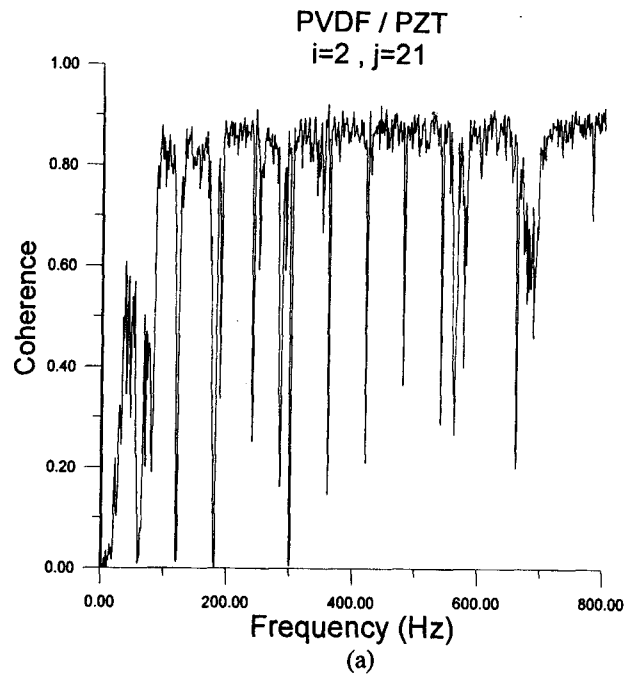

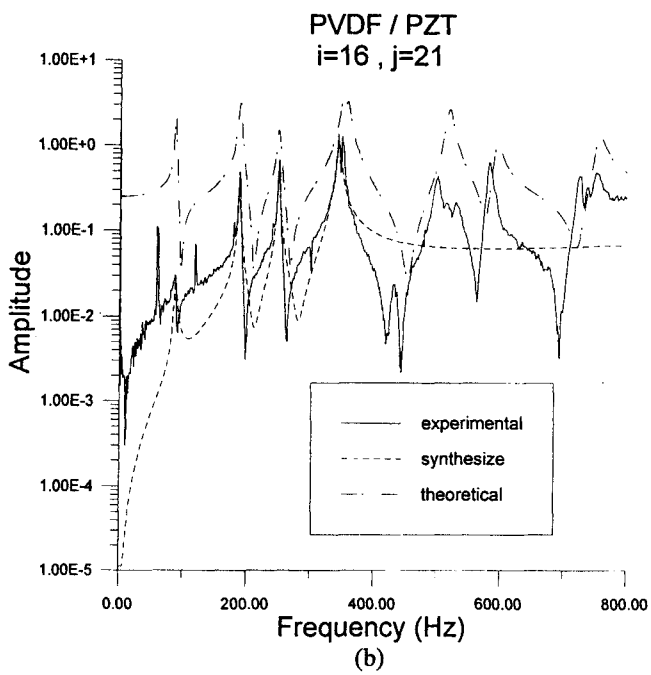

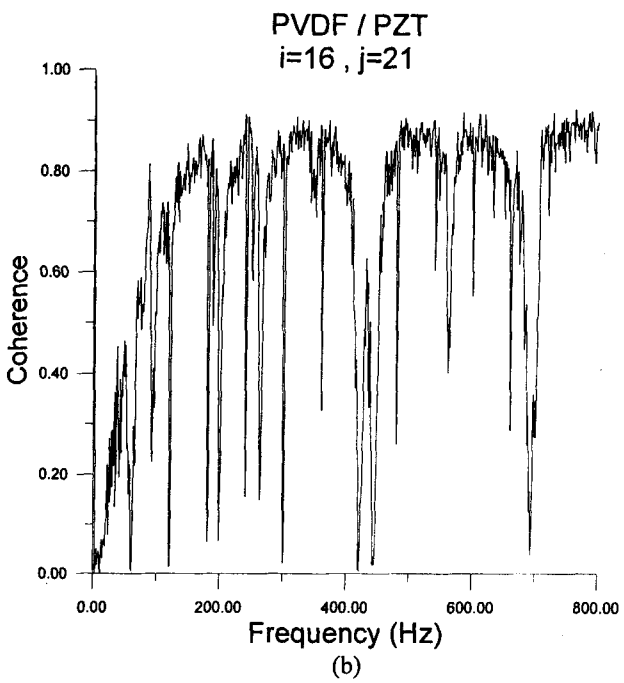

Figure 6. *Frequency response functions: (a)* i = 2, j = 21 *and (b)* i = 16, j = 21.

Figure 7. *Coherence functions: (a)* i = 2, j = 21 *and (b)* i = 16, j = 21.

Table 4. Natural frequencies of the simply supported plate (Hz).

m\n	1	2	3	4	5
1	87.71	249.81	519.98	898.22	1384.53
2	188.74	350.85	621.02	999.25	1485.56
3	357.13	519.23	789.40	1167.64	1653.95
4	592.88	754.98	1025.15	1403.39	1889.69
5	895.98	1058.08	1328.25	1706.48	2192.79

measurement of FRFs is satisfactory and suitable for further curve fitting process to extract modal parameters of the simply supported plate.

Verification of Modal Parameters

The measured FRFs are processed by adopting CADA-PC, a general modal parameter extraction software, to determine modal parameters of the simply supported plate. The results from the conventional modal testing by using hammer and accelerometer for the same plate conducted by the authors (Wang and Chen, 1997) are also cited for comparison. The simply supported plate is built based on the work by Ochs and Snowdion (1975).

Theoretical natural frequencies of the simply supported plate for $m = 5$, $n = 5$ are shown in Table 4. Table 5 shows the comparison of natural frequencies for the first five modes. One can observe that natural frequencies obtained from the conventional modal testing (ACC./Hammer) appear very good agreement less than ±3%. The test plate was fairly simulated for the simply supported boundary conditions (Wang and Chen, 1997). The extracted natural frequencies by the PVDF/PZT testing are smaller than that by the ACC./hammer testing. This may be due to the slight mass effect of piezoelectric transducers. The error percentage of the PVDF/PZT testing is less than –2.17%. As seen in Table 5, $f_{3,1} = 357.13$ Hz is closed to $f_{2,2} = 350.85$ Hz. This can cause modal coupling effect and will be discussed later. Piezoelectric transducers work well in predicting the natural frequencies of the structure.

Damping values can not be obtained through theoretical modal analysis. The viscous damping ratio is assumed to be 0.01 for all modes to generate the theoretical FRFs. The extracted modal damping ratios of the first four modes from the curve fitting process for both conventional (ACC./Hammer) and smart (PVDF/PZT) structural testings are also listed in Table 6. $\xi_{1,1}$ is 1.95% higher than the expected damping ratio 0.1–0.5% for steel material (Harris and Crede, 1976). Other modal damping ratios agree well. The damping ratios extracted from smart structural testing is generally slightly higher than that from a conventional one. It can be noted that the adhesion and material effect of the PZT patches and PVDF films can also contribute to increase damping but neglected in theoretical analysis.

Table 6. Comparison of modal damping ratios from experimental results.

	Damping Ratio (%)	
Damping Ratio	ACC./Hammer*	PVDF/PZT
$\xi_{1,1}$	2.24	1.95
$\xi_{1,1}$	0.15	0.39
$\xi_{1,2}$	0.16	0.35
$\xi_{2,2}$	0.47	0.78

*Results adopted from Wang and Chen (1997).

The first four theoretical displacement mode shapes of the simply supported plate are depicted in Figure 8, and the experimental PVDF sensor mode shapes are shown in Figure 9. Because the experimentally extracted mode shapes are complex number due to the damping effect, they are depicted in amplitude. All mode shape values shown in Figure 9 are positive. One can observe that there are certain degrees of similarity between Figures 8 and 9. In particular, for Figure 9(d) mode (2,2) there are two peak values near 1/3 of plate length in x-coordinate at central line of $y = 15$ cm. This can be explained that the natural frequency of (3,1) mode is 357.13 Hz near mode (2,2) 350.85 Hz. A modal coupling effect is observed. The PVDF sensor mode shapes as shown previously are proportional to the displacement mode shapes and validated in Figure 9. For comparison purpose, Figure 10 shows the experimentally extracted mode shapes from conventional structural modal testing (Wang and Chen, 1997) and reveals the similarity with Figure 9. The use of piezoceramic transducers for the experimental modal testing is demonstrated and shown promising.

MSF (modal scale factor) and MAC (modal assurance criterion) (Ewins, 1986) between the theoretical and experimentally predicted mode shapes are tabulated in Tables 7 and 8 respectively. One can see that the diagonal terms except for mode (2,2) close to one indicates the agreement between the

Table 5. Comparison of natural frequencies between theoretical and experimental results.

		Experimental (Hz)		Error Percentage (%)	
Natural Frequency	Theoretical (Hz)	ACC./Hammer*	PVDF/PZT	ACC./Hammer*	PVDF/PZT
$f_{1,1}$	87.71	90.12	88.43	2.75	0.82
$f_{2,1}$	188.74	189.96	188.44	0.65	–0.16
$f_{1,2}$	249.81	252.20	249.76	0.96	–0.02
$f_{2,2}$	350.85	341.23	343.22	–2.74	–2.17
$f_{3,1}$	357.13	—	—	—	—

*Results adopted from Wang and Chen (1997).

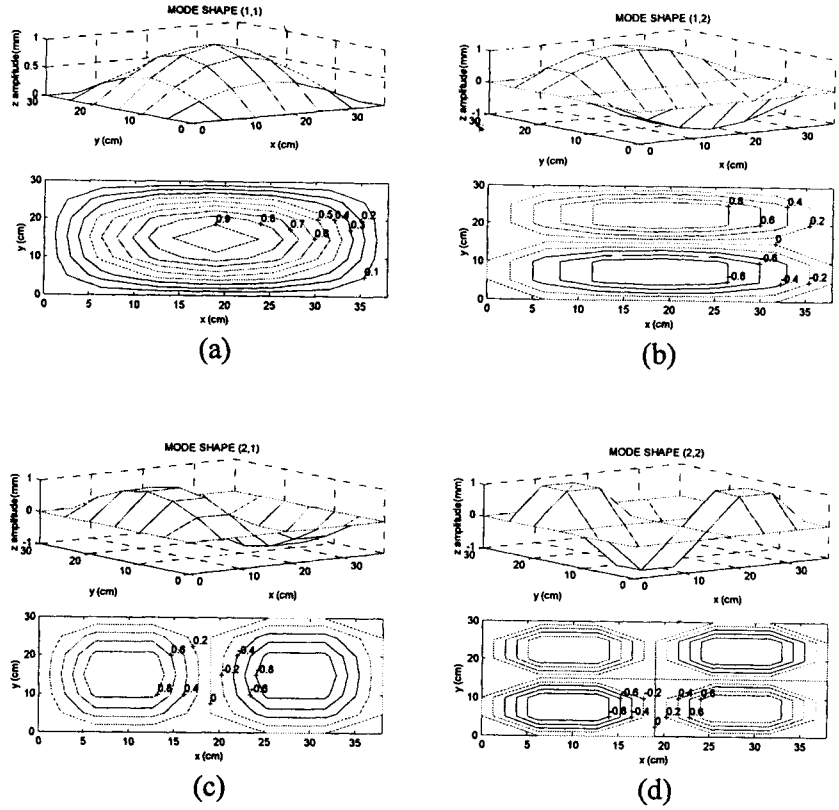

Figure 8. *Theoretical displacement mode shape of the simply supported plate: (a) (1,1) mode, (b) (1,2) mode, (c) (2,1) mode and (d) (2,2) mode.*

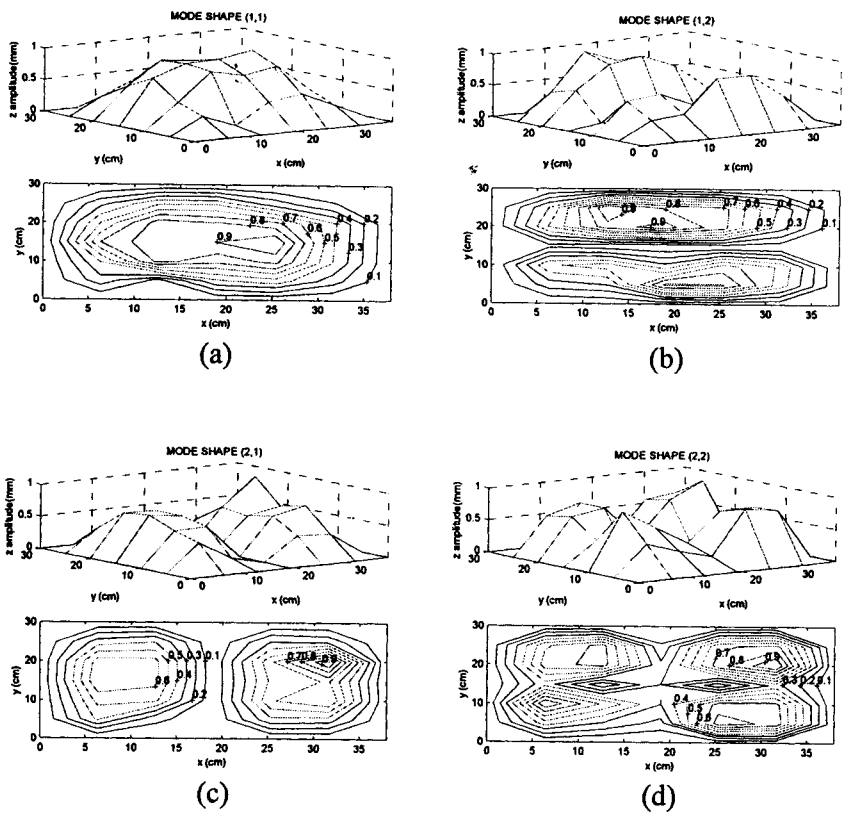

Figure 9. *Experimental PVDF sensor mode shape of the simply supported plane: (a) (1,1) mode, (b) (1,2) mode, (c) (2,1) mode and (d) (2,2) mode.*

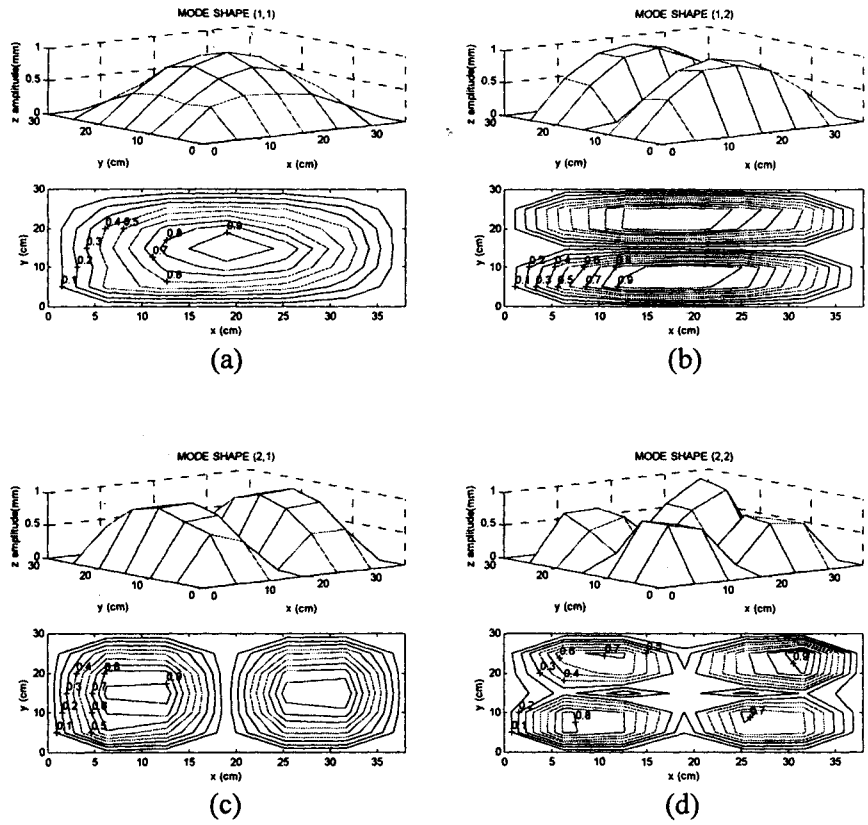

Figure 10. *Experimental hammer actuator mode shape of simply supported plate: (a) (1,1) mode, (b) (1,2) mode, (c) (2,1) mode and (d) (2,2) mode (Wang and Chen, 1997).*

theoretical and predicted mode shapes. The off-diagonal terms near zero indicate the orthogonality of mode shapes. The bad agreement of mode (2,2) is due to the coupling mode effect of mode (3,1) as discussed above. In summary, the use of PZT actuator incorporated with the PVDF sensors does successfully perform experimental modal testing of simply supported plate. The modal parameters, including natural frequencies, modal damping ratios and PVDF sensor mode shapes, are obtained and physically interpreted.

CONCLUSIONS

This work adopts the PZT actuator and PVDF sensors to perform smart structural modal testing for a simply supported plate. The theoretical modal analysis is first presented. The system frequency response function between the PZT actuator and PVDF sensor is also derived. The conventional experimental modal testing procedure is then performed with the use of piezoceramic transducers. A fixed PZT actuator and roving PVDF sensor to measure FRFs is used. Since FRFs can be expressed in conventional modal format, the traditional modal parameter extraction methods can be applied. All of the modal parameters, including natural frequencies, modal damping ratios and PVDF sensor mode shapes can be well identified and physically interpreted. In particular, the PVDF sensor mode shapes can be shown to be proportional to the displacement mode shapes. Through the comparison study of the FRFs and the extracted modal parameters to conventional modal testing, the idea of smart structural testing (SST) is demonstrated for its feasibility and validity. The major advantage of smart structural testing over the conventional structural testing is that the piezoceramic transducers can be integrated into the structure. The modal information can be useful for further applications in structural fault diagnosis. Numerous studies (Doebling et al., 1996; Farrar and Doebling, 1997) have been

Table 7. MSF (modal scale factor) values between theoretical and experimentally predicted mode shapes.

Mode	(1,1)	(2,1)	(1,2)	(2,2)
(1,1)	**0.9547+i0.0345**	−0.0125+i0.0691	0.0448−i0.0294	0.1075−i0.0556
(2,1)	0.0325−0.0089	**−0.9680+i0.0139**	−0.0597+i0.0055	−0.1111−i0.0593
(1,2)	0.1365+0.014	0.0984+i0.0086	**0.9469+i0.1294**	**−0.0374−i0.0291**
(2,2)	−0.0537+i0.0585	−0.0514−i0.0015	0.1524−i0.0012	−0.8257+0.3774

Table 8. MAC (modal assurance criterion) values between theoretical and experimentally predicted mode shapes.

Mode	(1,1)	(2,1)	(1,2)	(2,2)
(1,1)	**0.9114**	0.0002	0.0020	0.0116
(2,1)	0.0011	**0.9365**	0.0036	0.0123
(1,2)	0.0186	0.0097	**0.8967**	0.0014
(2,2)	0.0029	0.0026	0.0232	**0.6818**

dedicated to health monitoring and damage detection by the modal based method that is based on the modal parameter information. The model identification of the structure is also important to other applications such as structural vibration and acoustic control. The smart structure system can be enhanced for its future applications in structural fault diagnosis as well as structural vibration and acoustic control.

NOMENCLATURE

A_v = the PVDF sensor area
C_0 = geometric and material constants for both PZT patch and plate
$\bar{c}$ = damping coefficient per unit area
D = plate flexural stiffness
d_{31} = piezoelectric dielectric strain constant
E_p = Young's modulus of plate
e_{31}, e_{32}, e_{36} = piezoelectric field intensity constants
$f(x,y,t)$ = external force function
f_{mn} = the mn-th plate natural frequency (Hz)
$H(x)$ = step function
l_{cx}, l_{cy} = the length and width of the PZT actuator
l_{vx}, l_{vy} = the length and width of the PVDF film
L_x, L_y = the length and width of the plate
M_{eq} = equivalent line moment induced by the pure bending PZT actuator
$q(t)$ = charge output of PVDF sensor
t_c = thickness of PZT patch
t_p = plate thickness
t_v = thickness of the PVDF film
V_{c_j} = the input voltage of the j-th PZT
V_{v_i} = the output voltage of the i-th PVDF
w = transverse displacement of plate
x_{c_j}, y_{c_j} = the central location of the j-th PZT actuator in x- and y-coordinates
x_{v_i}, y_{v_i} = the central location of the i-th PVDF sensor in x- and y-coordinates
x_{c1_j}, x_{c2_j} = the location of the j-th PZT actuator in x-coordinates
x_{v1_i}, x_{v2_i} = the location of the i-th PVDF sensor in x-coordinates
y_{c1_j}, y_{c2_j} = the location of the j-th PZT actuator in both y-coordinates
y_{v1_i}, y_{v2_i} = the location of the i-th PVDF sensor in y-coordinates
$\delta(x)$ = delta function
ε = the permittivity of PVDF film
Λ = the free strain of piezoelectric actuator
ϕ_{mn} = the mn-th displacement mode shape
$\phi^c_{mn,j}$ = the mn-th PZT mode shape function at the j-th location of the PZT actuator
$\phi^v_{mn,i}$ = the mn-th PVDF mode shape function at the i-th location of the PVDF sensor
$\Gamma(x,y)$ = shape function of the PVDF film sensor
ν = Poisson's ratio of plate
ρ = plate density
ω_{mn} = the mn-th plate natural frequency (rad/sec)
ξ_{mn} = the mn-th modal damping ratio

ACKNOWLEDGEMENTS

The authors gratefully thank the financial support for this work from National Science Council of Republic of China under contract number: NSC89-2212-E-020-001.

REFERENCES

Bailey, T. and J. E. Hubbard, 1985, "Distributed Piezoelectric-Polymer Active Vibration Control of a Cantilever Beam," *AIAA Journal of Guidance Control,* 6: 605–611.

Clark, R. L. and C. R. Fuller, 1992, "A Model Reference Approach for Implementing Active Structural Acoustic Control," *Journal of Acoustical Society of America,* 6: 1534–1544.

Clark, R. L., C. R. Fuller and A. Wicks, 1991, "Characterization of Multiple Piezoelectric Actuators for Structural Excitation," *Journal of Acoustical Society of America,* 90: 346–357.

Clark, R. L., R. A. Burdisso and C. R. Fuller, 1993, "Design Approaches for Shaping Polyvinylidene Fluoride Sensors in Active Structural Acoustic Control," *Journal of Intelligent Material System and Structures,* 4: 354–365.

Collet, M. and L. Jezequel, 1994, "A New Approach to Modal Filtering with Laminated Piezo-electric Sensors," *Proceedings of the 12th International Modal Analysis Conference,* 246–254.

Collins, S. A., C. E. Padilla, R. J. Notestine, A. H. von Flotow, E. Schmitz and M. Ramey, 1992, "Design, Manufacture, and Application to Space Robotics of Distributed Piezoelectric Film Sensors," *Journal of Guidance Control,* 15: 396–403.

Crawley, E. F. and J. de Luis, 1987, "Use of Piezoelectric Actuators as Elements of Intelligent Structures," *AIAA Journal,* 25(10): 1373–1385.

D'Cruz, J., 1993, "The Active Control of Panel Vibrations with Piezoelectric Actuators," *Journal of Intelligent Material Systems and Structures,* 4: 398–402.

Dimitriadis, E. F., C. R. Fuller and C. A. Rogers, 1991, "Piezoelectric Actuators for Distributed Vibration Excitation of Thin Plates," *Transactions of the ASME,* 113: 100–107.

Doebling, S. W., C. R. Farrar, M. B. Prime and D. W. Shevitz, 1996, "Damage Identification and Health Monitoring of Structural and Mechanical Systems from Changes in their Vibration Characteristics: A Literature Review," *Los Alamos National Laboratory Report:* LA-13070-MS.

Ewins, D. J., 1986, *Modal Testing: Theory and Practice,* Research Studies Press LTD., Letchworth Hertfordshire, England.

Farrar, C. R. and S. W. Doebling, 1996, "An Overview of Modal-Based Damage Identification Methods," *Los Alamos National Laboratory Report.*

Galea, S. C., W. K. Chiu and J. J. Paul, 1993, "Use of Piezoelectric Films in Detecting and Monitoring Damage in Composites," *Journal of Intelligent Material Systems and Structures,* 4: 330–336.

Gibbs, G. P., and C. R. Fuller, 1992, "Excitation of Thin Beams Using Asymmetric Piezoelectric Actuators," *Journal of Acoustical Society of America,* 92(6): 3221–3227.

Harris, C. M. and C. E. Crede, 1976, *Shock and Vibration Handbook,* McGraw-Hill Inc.

Huang, J. K., C. H. Choi, C. K. Song and J. M. Lee, 1998, "Identification of a Thin Plate with Piezoelectric Actuators and Sensors," *Journal of Vibration and Acoustics,* 120: 826–828.

Hubbard, J. E., 1987, "Distributed Sensors and Actuators for Vibration Control in Elastic Components," *Noise-Con,* 87, 407–412.

Im, S. and S. N. Atluri, 1989, "Effects of a Piezo-Actuator on a Finitely Deformed Beam Subjected to General Loading," *AIAA Journal,* 27(12): 1801–1807.

Lee, C. K. and F. C. Moon, 1990, "Modal Sensors/Actuators," *Journal of Applied Mechanics,* 57: 434–441.

Norwood, C., 1995, "The Measurement of Natural Frequencies and Mode Shapes of Submerged Cylinders Using PVDF Strip Excitation," *Proceedings of Inter-Noise,* 95, 1337–1340.

Ochs, J. B. and J. C. Snowdion, 1975, "Transmissibility Across Simply Supported Thin Plates. I. Rectangular and Square Plates with and without Damping Layers," *Journal of Acoustical Society of America,* 58(4): 832–840.

Plump, J. M., J. E. Hubbard and T. Bailey, 1987, "Nonlinear Control of a Distributed System: Simulation and Experimental Results," *Journal of Dynamic System, Measurement, and Control,* 109: 133–139.

Sun, F. P., C. Liang and C. A. Rogers, 1994, "Experimental Modal Testing Using Piezoceramic Patches as Collocated Sensor-Actuators," *Proceedings of the 1994 SEM Spring Conference and Exhibits,* 871–879.

Szilard, R., 1974, *Theory and Analysis of Plates Classical and Numerical Methods,* Prentice Hall, Inc., Englewood Cliffs, New Jersey.

Tanaka, N., S. D. Snyder and C. H. Hansen, 1996, "Distributed Parameter Modal Filtering Using Smart Sensors," *Transactions of the ASME Journal of Vibration and Acoustics,* 118:630–640.

Wang, B. T., 1994, "Active Control of Far-Field Sound Radiation by a Beam: Physical System Analysis," *Smart Materials Structures,* 3: 476–484.

Wang, B. T., 1996, "Characterization of Transfer Functions for Piezoceramic and Conventional Transducers," *Journal of Intelligent Material Systems and Structures,* 7: 390–398.

Wang, B. T., 1998, "Structural Modal Testing with Various Actuators and Sensors," *Mechanical Systems and Signal Processing,* 12(5): 627–639.

Wang, B. T. and C. A. Rogers, 1991a, "Laminate Plate Theory for Spatially Distributed Induced Strain Actuators," *Journal of Composite Materials,* 25: 433–452.

Wang, B. T. and C. A. Rogers, 1991b, "Modeling of Finite-Length Spatially Distributed Induced Strain Actuators for Laminate Beams Structures," *Journal of Intelligent Material Systems and Structures,* 2: 38–58.

Wang, B. T. and C. C. Wang, 1997, "Feasibility Analysis of Using Piezoceramic Transducers for Cantilever Beam Modal Testing," *Smart Materials Structures,* 6:106–116.

Wang, B. T. and R. L. Chen, 1997, "Experimental Modal Analysis of a Simply Supported Plate," *Bulletin of National Pingtung University of Science and Technology,* (in Chinese) 6(4): 273–281.

Young, A. J. and C. H. Hansen, 1994, "Control of Flexural Vibration in a Beam Using a Piezoceramic Actuator and an Angle Stiffener," *Journal of Intelligent Material Systems and Structures,* 5: 536–549.